Pure Appl. Opt. **7** (1998) 1237–1248. Printed in the UK PII: S0963-9659(98)90568-2

Annular focusing through a dielectric interface: scanning and confining the intensity

S H Wiersma†, T D Visser†§ and P Török‡

† Department of Physics and Astronomy, Free University, De Boelelaan 1081, 1081 HV Amsterdam, The Netherlands

‡ Department of Engineering Science, University of Oxford, Parks Road, Oxford OX1 3PJ, UK

Received 9 January 1998, in final form 11 May 1998

Abstract. We study the problem of light focusing by a high-aperture lens through a planar interface between two media with different refractive indices. It is demonstrated how, by using annular illumination, the intensity distribution can be significantly confined. A new scanning mechanism is proposed to continuously probe the intensity peak through the second medium. This mechanism may be applied in, for example, lithography and three-dimensional imaging.

1. Introduction

The influence of a plane dielectric interface on a converging spherical wave has been studied recently by several groups. Török *et al* [1] use an angular spectrum representation in the Debye approximation. Wiersma and Visser [2] employ the so-called m-theory. Dhayalan and Stamnes [3] also use a plane-wave decomposition, but without the Debye approximation. Both [1] and [2] take the classic papers by Wolf [4] and Richards and Wolf [5] as a starting point. Although the analysis in [1] is very different from that in [2], it was found that the numerical results of both studies are in good agreement [6]. (Note that this comparison was for high Fresnel number systems, outside the regime of the focal shift phenomenon.) Other studies dealing with the effect of a dielectric interface are [7–10].

Focusing through a dielectric interface introduces spherical aberration. The aberrated wavefront may be expanded in terms of, for example, Zernike polynomials [11]. Spherical aberration may be suppressed by counterbalancing the terms in the expansion. This is the basis of adaptive optics and phase mask techniques which are both used to compensate optical path differences. It has, however, been shown by Török *et al* [12] that interface focusing introduces higher-order aberration terms which are likely to be difficult to correct by means of adaptive optics. For the same reason spherical aberration caused by interface focusing cannot be fully compensated by altering the tubelength of a lens [13] because this only compensates for lower-order aberration terms.

A third possibility to reduce aberrations is to use annular illumination rather than an unobscured lens. It is the aim of this paper to explore this option.

Note that a phase mask is optimized for only one focusing depth, whilst adaptive optics solutions such as an annulus can, at least in principle, be varied in a continuous manner. As will be explained, this allows one to scan the intensity through the second medium.

§ Author to whom correspondence should be addressed.

The analysis in this paper is fully vectorial. However, in order to gain physical insight, a geometrical optics analysis is presented in the appendix.

In the examples we use refractive indices (n) rather than permittivities (ϵ). The relation between the two is $n^2 = \epsilon_r$, with $\epsilon_r = \epsilon/\epsilon_0$, where ϵ_r is the relative permittivity and ϵ_0 is the permittivity *in vacuo*.

In this paper we are concerned with the time-averaged electric energy density, hereafter simply called 'the intensity'.

2. The effect of an interface on an unobscured focused beam

The geometry of our problem is depicted in figure 1. A lens focuses an incident, linearly polarized, plane wave through a dielectric interface. The interface is perpendicular to the direction of propagation ($-z$). For the calculations in this section the results of [2] are used.

If there is no interface (i.e. $n_1 = n_2$), then an increasing semi-aperture angle Ω_1 will result in a decreasing width of the peak of the axial intensity distribution, as is shown in figure 2. This situation changes completely when an interface is present. As is seen in figure 3, the axial distribution for $\Omega_1 = 45^\circ$ is highly asymmetric and has a jagged appearance. For a *smaller* aperture angle, namely $\Omega_1 = 20^\circ$, the distribution is now much narrower. However, for $\Omega_1 = 10^\circ$ it is seen that the peak is wider again. So, it seems that for a given configuration there exists an optimum value of the semi-aperture angle for which the axial diffraction pattern is the most localized. This can be understood by realizing that there are two competing processes at work. An increasing numerical aperture decreases the axial resolution as in figure 2. At the same time, however, an increasing aperture angle causes an increasing phase difference between the secondary Huygens sources at the interface, giving rise to a widening of the axial diffraction pattern [14].

The broadening of the intensity distribution due to an interface (which increases with increasing focusing depth) has major implications for three-dimensional imaging (see also

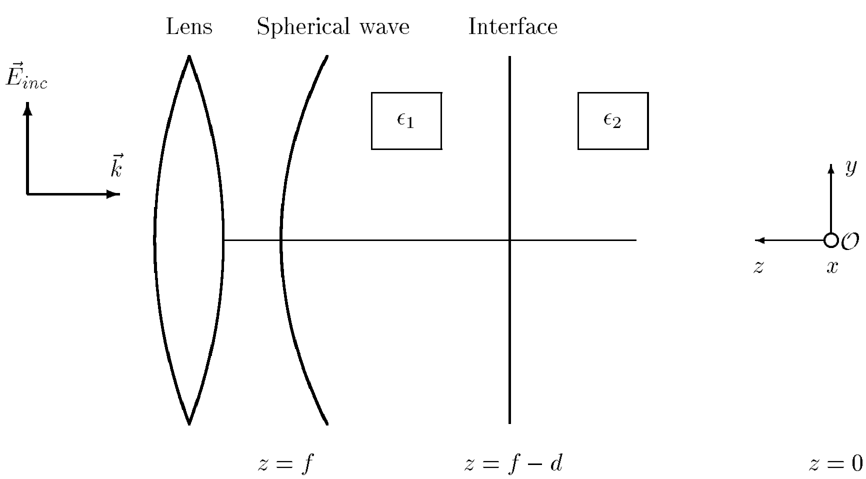

Figure 1. Geometry of the system. A linearly polarized plane wave is converted by a lens with focal length f and semi-aperture angle Ω_1 into a converging spherical wave. The medium left of the interface has permittivity ϵ_1, the medium to the right of the interface has permittivity ϵ_2. Both media are assumed to be non-magnetic ($\mu = \mu_0$) and non-conducting ($\sigma = 0$). The system is symmetric with respect to rotations around the z-axis.

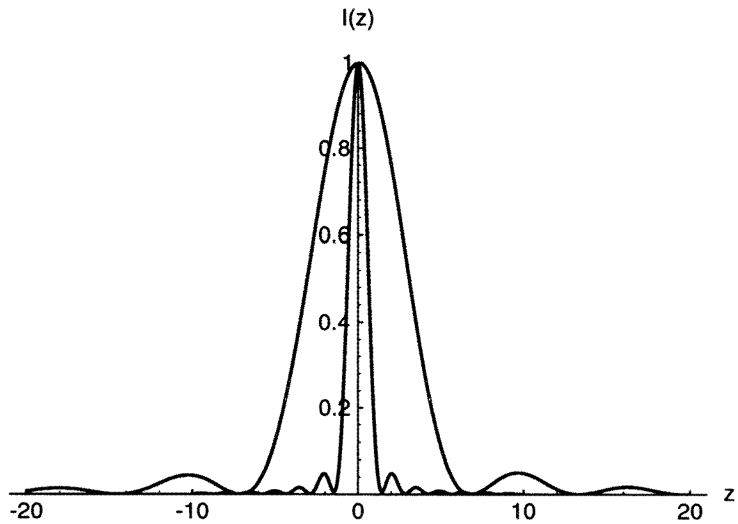

Figure 2. Intensity distribution along the z-axis (in μm) for two semi-aperture angles when $n_1 = n_2$. The narrow peak is for $\Omega_1 = 45°$, the broad distribution is for $\Omega_1 = 20°$. The other parameters in both cases are $\lambda_0 = 632.8$ nm, $n_1 = n_2 = 1.51$, $f = 10^{-2}$ m.

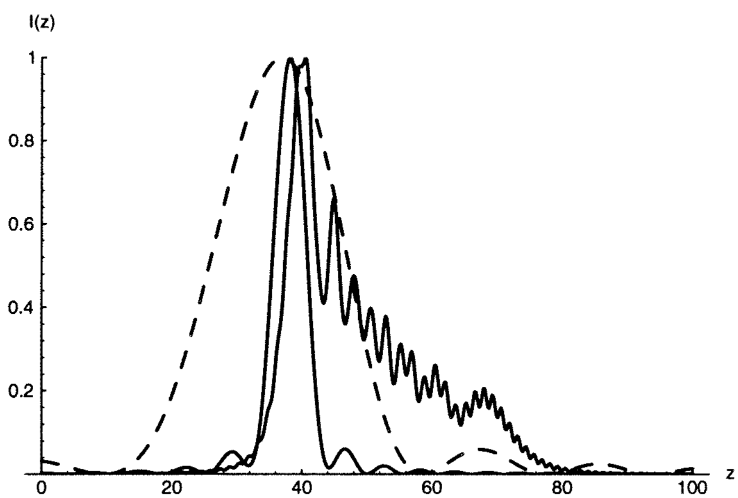

Figure 3. Comparison of the intensity distribution along the z-axis (in μm) for three different semi-aperture angles. The wide symmetric peak is for $\Omega_1 = 10°$ (broken curve), the narrow symmetric peak is for $\Omega_1 = 20°$, and the broad, jagged distribution is for $\Omega_1 = 45°$. The other parameters in all cases are $\lambda_0 = 632.8$ nm, $n_1 = 1.51$, $n_2 = 1.33$, $f - d = 300$ μm, $f = 10^{-2}$ m.

section 6 of [6], [15, 16]). For confocal microscopy, where high numerical aperture oil-immersion lenses with $n_{\mathrm{oil}} = 1.51$ are commonly used to study biomedical objects with $n_{\mathrm{water}} = 1.33$, this dependence of the peak width on Ω_1 indicates that lower aperture angles can improve the optical sectioning capabilities.

3. Stationary phase and geometrical optics

In [2] it was derived that for an unobscured lens the axial electric field in the second medium is given by

$$E_x(z) = C(z) \int_0^{\Omega_1} \mathrm{e}^{\mathrm{i}k_2 s - \mathrm{i}k_1 t}\, g(\theta_1, z)\ \mathrm{d}\theta_1 \tag{1}$$

with

$$C(z) = \tfrac{1}{2} f (f-d)^2 \left(\frac{z}{f-d} - 1 \right) \exp(\mathrm{i}k_1 f) \tag{2}$$

$$g(\theta_1, z) = \left(\frac{1}{s^3} - \frac{\mathrm{i}k_2}{s^2} \right) \left(\eta_s + \eta_p \cos\theta_2 \right) \tan\theta_1. \tag{3}$$

The subscript x in equation (1) indicates that the incident plane wave is linearly polarized along the x-direction. Also, $f - d$ is the distance between the focus of the lens and the interface, k_i $(i = 1, 2)$ is the wavenumber in medium i, η_s and η_p are Fresnel transmission coefficients. The angle θ_2 follows from θ_1 through Snell's law. The functions s and t are defined as

$$t(\theta_1) = \frac{f-d}{\cos\theta_1} \tag{4}$$

$$s(\theta_1) = \left(t^2 + z^2 - 2z(f-d) \right)^{1/2}. \tag{5}$$

In order to get more insight into the physics of the situation, we now develop a stationary phase analysis of this integral [8]. The phase of the exponent in equation (1) is stationary if

$$\frac{\mathrm{d}}{\mathrm{d}\theta_1} (k_2 s - k_1 t) = 0 \tag{6}$$

which is readily translated into

$$\left(k_2 \frac{t}{s} - k_1 \right) \frac{\mathrm{d}t}{\mathrm{d}\theta_1} = 0. \tag{7}$$

For $f \neq d$, one solution is $\mathrm{d}t/\mathrm{d}\theta_1 = 0$. From equation (4) it follows that this is for $\theta_1 = 0$. However, since the amplitude function $g(\theta_1 = 0) = 0$, this stationary endpoint yields a contribution of order $1/k$ to the integral and is neglected. The contribution of the non-stationary endpoint at $\theta_1 = \Omega_1$ is also of order $1/k$, and is neglected too. Another solution is

$$k_2 t = k_1 s. \tag{8}$$

Using that $k_i = n_i k_0$, with $i = 1, 2$ and k_0 the wavenumber *in vacuo* together with equations (4) and (5) this gives

$$\frac{z^2}{t^2} - 2\frac{z}{t}\cos\theta_1 + 1 - \frac{n_2^2}{n_1^2} = 0. \tag{9}$$

Solving this for z/t yields

$$\frac{z}{t} = \cos\theta_1 \pm \sqrt{\cos^2\theta_1 - 1 + \left(\frac{n_2}{n_1} \right)^2} \tag{10}$$

$$= \cos\theta_1 \pm \frac{n_2}{n_1} \sqrt{1 - \sin^2\theta_2} \tag{11}$$

$$= \cos\theta_1 \pm \frac{n_2}{n_1} \cos\theta_2. \tag{12}$$

Using equation (12) together with equation (4) gives

$$z = f - d \pm \frac{n_2}{n_1}(f - d)\frac{\cos\theta_2}{\cos\theta_1}. \tag{13}$$

Defining the *positive* depth h below the interface as

$$h = f - d - z \tag{14}$$

gives

$$h = (f - d)\frac{n_2}{n_1}\frac{\cos\theta_2}{\cos\theta_1}. \tag{15}$$

Equation (15) expresses a relation between the axial position h and the angle θ_1 which gives the main contribution to the integral of equation (1). This is exactly equation (A3) of the appendix which was derived using Snell's law. This is an illustration of the fact that for $k \to \infty$ (as is implicitly assumed in stationary phase analysis) wave optics reduces to geometrical optics. It also means that the main contribution to the asymptotic expansion of equation (1) vanishes outside the so-called geometrical shadow boundaries (see also the appendix).

We continue the analysis of equation (1) by squaring condition (15) and re-writing it as

$$\sin\theta_s(z) = \left[\frac{h^2 - (f - d)^2(n_2/n_1)^2}{h^2 - (f - d)^2}\right]^{1/2} \tag{16}$$

where the subscript s indicates the value of θ_1 for which the phase is stationary at position z. Equation (16) represents an interior stationary point. Hence, the asymptotic expansion of equation (1) is given in first order as [8, 17]

$$E_x(z) \sim \left[\frac{2\pi}{|k_2 s''(\theta_s) - k_1 t''(\theta_s)|}\right]^{1/2} g(\theta_s, z)\, C(z)\, \mathrm{e}^{\mathrm{i}(k_2 s(\theta_s) - k_1 t(\theta_s))}\, \mathrm{e}^{\pm \mathrm{i}\pi/4}. \tag{17}$$

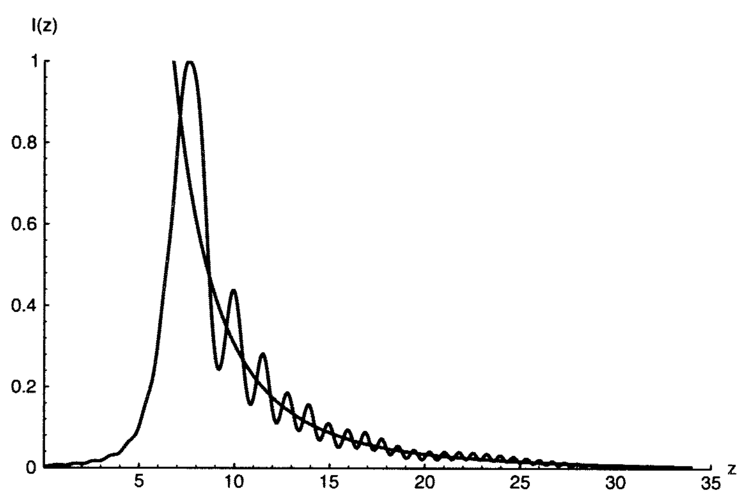

Figure 4. Comparison of an asymptotic approximation (smooth curve) and the exact expression (jagged curve) for the axial intensity. In this example $\lambda_0 = 0.632.8\ \mu$m, $\Omega = 60^\circ$, $f - d = 50\ \mu$m, $n_1 = 1.51$, $n_2 = 1.33$.

Here the upper (lower) sign is taken according as to whether $k_2 s''(\theta_s) - k_1 t''(\theta_s)$ is greater (smaller) than zero. Also, using condition (8),

$$k_2 s''(\theta_s) - k_1 t''(\theta_s) = \frac{k_2}{s}\left[1 - \frac{k_1^2}{k_2^2}\right] t'^2. \tag{18}$$

So, for the intensity we find

$$I(z) = \tfrac{1}{4}\epsilon_2 |E(z)|^2 \tag{19}$$

$$\sim \frac{\epsilon_2 \pi s(\theta_s)}{2k_2 |1 - (k_1/k_2)^2| t'(\theta_s)^2} |g(z)\, C(z)|^2. \tag{20}$$

A comparison of the exact expression equation (1) and the asymptotic approximation equation (20) is depicted in figure 4. Note that the first-order approximation shows no interference pattern. Also, in contrast to the exact solution, it is discontinuous at the left-hand geometrical shadow boundary. Finally, the asymptotic expression slightly displaces the maximum.

4. Annular illumination: localizing the intensity

In figure 4 it is seen that the intensity distribution can have many secondary maxima. Just as by decreasing the semi-aperture angle (figure 3), we can reduce the number of maxima by using an annular aperture. This has the additional advantage that the light can be 'aimed' to have a peak around any axial position z, provided that z lies between the geometrical shadow boundaries of the unobscured lens.

For a given configuration (i.e. the set of parameters Ω_1, f, d, λ_0, n_1 and n_2) one can find for any position z between the shadow boundaries the value of $\theta_s(z)$ through equation (16). From the considerations of the previous section, it follows that by restricting the illumination to an interval around $\theta_s(z)$ most of the intensity will be found in the vicinity

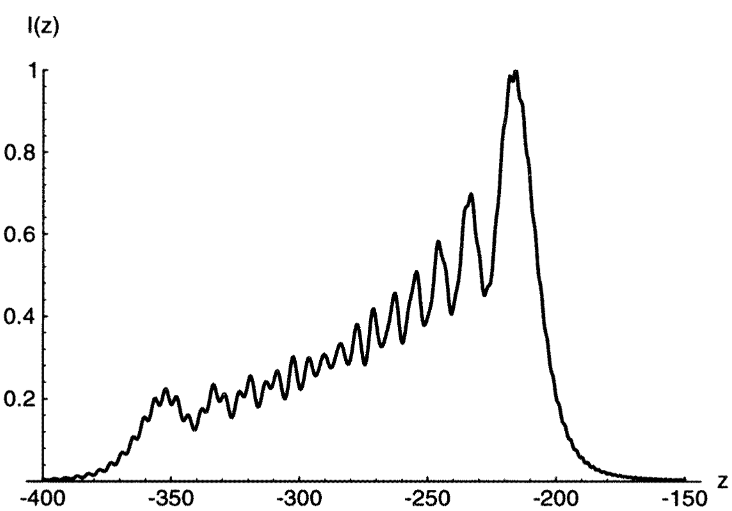

Figure 5. Intensity distributions along the z-axis (in μm) for an unobscured lens. $\lambda_0 = 0.6328\ \mu$m, $\Omega_1 = 50°$, $f = 10^{-2}$ m, $f - d = 200\ \mu$m, $n_1 = 1.00$, $n_2 = 2.00$. Note that the peak intensity here corresponds to 2.9% of the peak intensity of the case $n_1 = n_2 = 1.00$.

of z. (In practice, the annulus can be placed at different positions: at the back focal plane [18], at the exit pupil or at the dielectric interface.) To illustrate this, consider the axial diffraction pattern for an unobscured lens shown in figure 5. The intensity distribution is relatively spread out, and exhibits many secondary peaks. It was found that the peak intensity in this case is 2.9% of that which occurs for $n_1 = n_2 = 1.00$ (keeping all other parameters fixed).

Suppose now that we want to concentrate the intensity around the secondary peak at $z = -302.3\ \mu$m. For this particular configuration $\theta_s(z = -302.3\ \mu\text{m}) = 41.2^\circ$, according to equation (16). By using an annulus around this value, the light can indeed be localized around the prescribed z value. The dependence of $I(z)$ on the annular interval limits θ_{low} and θ_{high} is depicted in figure 6. The optimized interval (i.e. giving the highest intensity) is determined numerically. The intensity distribution for this annulus is shown in figure 7 (left-hand curve). A sharply enhanced (51%) single peak centred around $z = -302.3\ \mu$m is indeed obtained. Also, the number of secondary maxima and their heights are both strongly reduced. If we change the annulus, the intensity peak can be shifted to, for example, $z = -246\ \mu$m (right-hand curve). We conclude that by adjusting the annulus we can 'aim' the light to be focused anywhere between the geometrical shadow boundaries. Note that one can also localize the intensity around the peak of the distribution for the unobscured lens (i.e. at $z = -215\ \mu$m in figure 5).

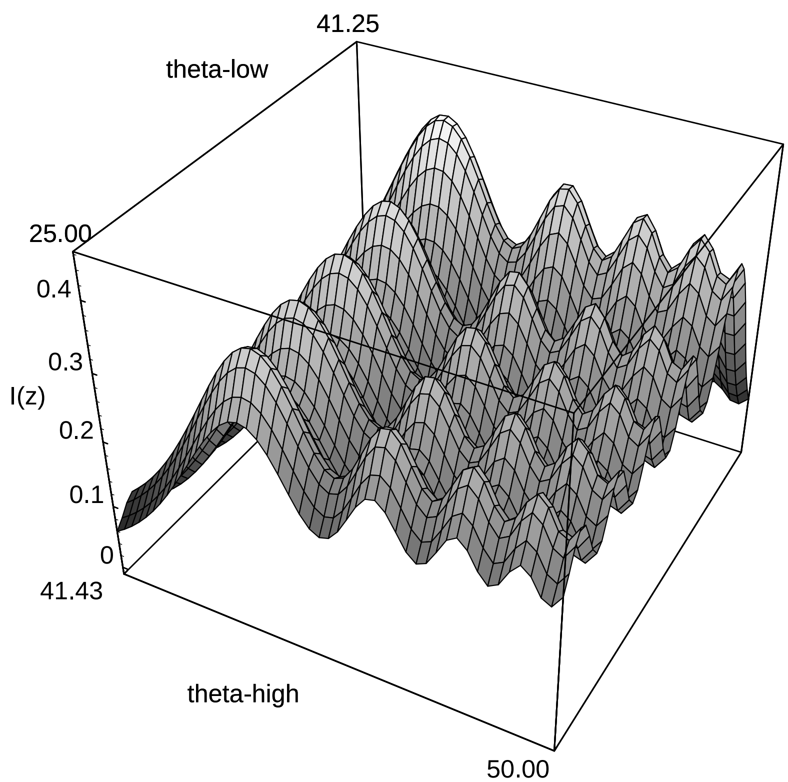

Figure 6. The intensity I ($z = -302.3\ \mu$m) as a function of the angular interval limits θ_{low} and θ_{high}. All parameters are as in figure 5.

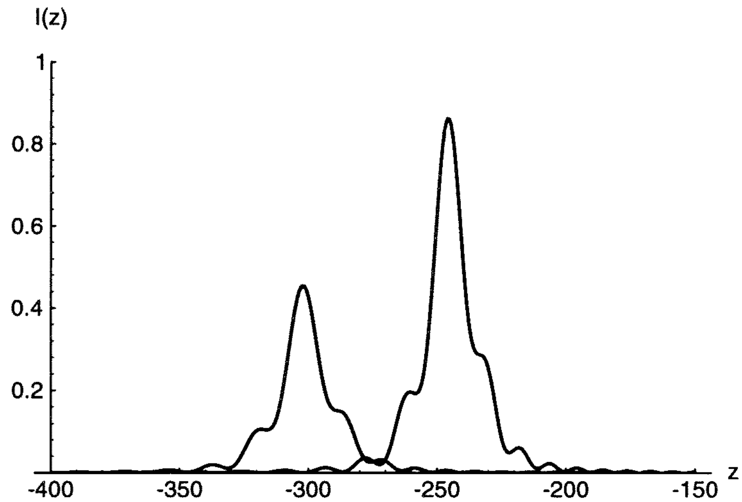

Figure 7. Intensity distributions along the z-axis (in μm) for the optimized annuli [37.8°, 44.2°] (left-hand curve) and [23.6°, 34.3°] (right-hand curve). The peak intensity is increased by 51% and 48%, respectively. All parameters are as in figure 5.

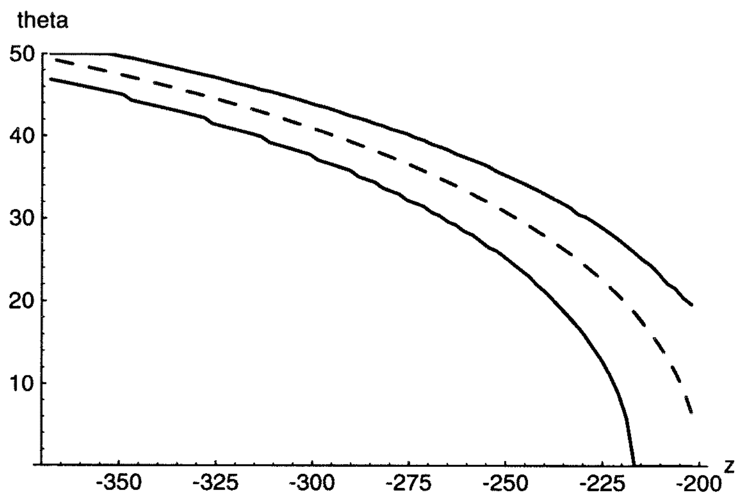

Figure 8. The stationary phase θ_{stat} (broken curve), and the two interval limits θ_{low} (lower curve) and θ_{high} (upper curve) which give an optimal intensity as a function of the axial position z (in μm). All parameters are as in figure 5.

The optimized values of θ_{low} and θ_{high} as a function of z are depicted in figure 8. The optimal angular interval always includes the stationary phase angle $\theta_s(z)$. Note that θ_{low} suddenly becomes nonzero around the position of the original maximum. This is related to the fact that the paraxial rays, which together make up the maximum peak for the case of an unobscured lens, gradually get out of phase with the rays around $\theta_{stat}(z)$ as z becomes more negative. Therefore, from a certain z-value onwards, these paraxial rays are no longer part of the optimized annulus. Also, it is seen that from certain z-values on $\theta_{high} = 50°$. This is due to the fact that θ_{high} cannot exceed Ω_1.

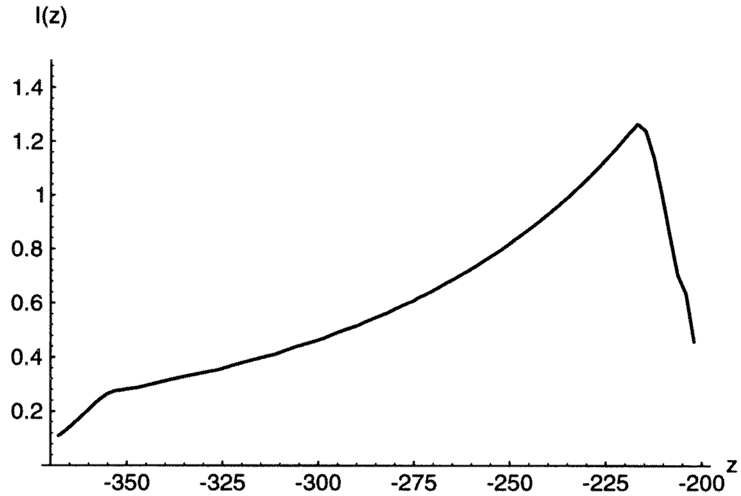

Figure 9. The maximum intensity that can be obtained by optimizing the annulus, as a function of the axial position z (in μm). The normalization, as well as all other parameters, is as in figure 5.

The maximum intensity, as produced by optimizing the angular interval, is shown in figure 9. Note that, although this is a smooth distribution, the general form of the diffraction pattern in figure 5 can still be recognized. For certain applications it may be desirable to have a constant peak intensity while scanning through the second medium. The curve in figure 9 indicates how the incident power should be adjusted as a function of z to obtain this.

5. Conclusions

We have analysed the effect of a plane dielectric interface on a converging spherical wave. A relation between the requirement of stationary phase and the geometrical description of the focusing process was established.

It was found that by using a well chosen annulus the axial intensity distribution can be significantly confined, and the secondary maxima strongly suppressed. Moreover, the local intensity can be increased in this manner.

It was shown how by continuously varying the annulus and the input power, a constant intensity peak can be scanned axially (within certain limits) through the second medium. This new scanning method has possible applications in, for example, three-dimensional imaging and lithography.

Appendix. Geometrical optics analysis

In this appendix we analyse our problem from a geometrical optics point of view. We discuss the axial focal displacement associated with the aberration caused by the interface, and the so-called geometrical shadow boundaries. The latter are relevant for the stationary phase analysis of section 3.

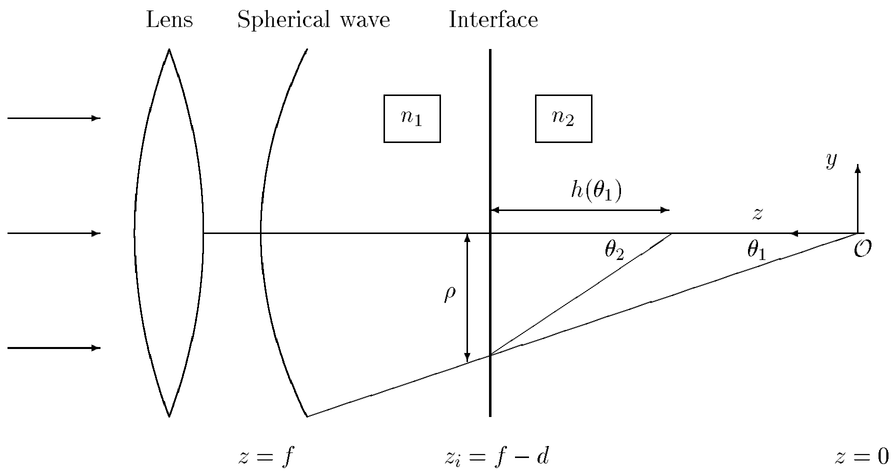

Figure A1. Ray tracing for focusing through an interface. A lens with focal length f and semi-aperture angle Ω_1 is placed at a distance d in front of an interface between two media. A typical ray which is incident under an angle θ_1 passes the interface at a distance ρ from the z-axis. After refraction, it crosses the axis at a distance h from the interface.

Let ρ denote the distance from the z-axis at which a ray incident under an angle θ_1 crosses the interface (see figure A1). We then have

$$\tan\theta_1 = \frac{\rho}{f - d}. \tag{A1}$$

If the refracted ray makes an angle $\theta_2 = \arcsin(n_1 \sin\theta_1/n_2)$ with the z-axis, then

$$\tan\theta_2 = \frac{\rho}{h(\theta_1)}. \tag{A2}$$

Here $h(\theta_1)$ is the distance between the interface and the point where the refracted ray crosses the z-axis. Eliminating ρ gives

$$h(\theta_1) = (f - d)\frac{\tan\theta_1}{\tan\theta_2} = (f - d)\frac{n_2}{n_1}\frac{\cos\theta_2}{\cos\theta_1} \qquad 0 < \theta_1 \leqslant \Omega_1. \tag{A3}$$

(Note that this expression does not hold for the ray incident at $\theta_1 = 0$.) From figure A1 it is clear that the refracted ray crosses the z-axis at $z = f - d - h(\theta_1)$. In other words, the interface introduces an axial focal displacement $\Delta_f(\theta_1)$ of

$$\Delta_f(\theta_1) = (f - d)\left(1 - \frac{n_2\cos\theta_2}{n_1\cos\theta_1}\right). \tag{A4}$$

For $n_1 = n_2$ there is no focal displacement. In that case equation (A4) reduces to $\Delta_f = 0$, as expected.

In contrast to diffraction theory, geometrical optics predicts that the intensity distribution is confined to a finite part of the z-axis in the second medium. Equation (A3) defines two ‘shadow boundaries’ on the z-axis between which the intensity is concentrated. Although, as remarked above, this equation does not hold for $\theta_1 = 0$, this ray corresponds to an infinitely small area of the incident beam, its contribution to the intensity distribution is negligible. Therefore, these shadow boundaries, a marginal one z_m and a paraxial one z_p, are at

$$z_m = f - d - h(\Omega_1), \tag{A5}$$

$$z_p = f - d - \lim_{\theta_1 \downarrow 0} h(\theta_1) = (f - d)\left(1 - \frac{n_2}{n_1}\right). \tag{A6}$$

Note that for $n_2 \neq n_1$ both z_p and z_m are finite. The above derivation is only valid if no total internal reflection takes place and we may hence use Snell's law.

Every point z on the optical axis within the shadow boundaries corresponds to a single value of θ_1. In order to determine this inverse relation, equation (A3) is squared to obtain

$$h^2\big(1 - \sin^2\theta_1\big) = (f - d)^2\left(\frac{n_2}{n_1}\right)^2\left[1 - \left(\frac{n_1}{n_2}\right)^2 \sin^2\theta_1\right] \tag{A7}$$

or

$$\sin^2\theta_1(h) = \left[(f - d)^2\left(\frac{n_2}{n_1}\right)^2 - h^2\right] \Big/ \big[(f - d)^2 - h^2\big]. \tag{A8}$$

Using that $h = f - d - z$ (see figure A1) we finally find that

$$\theta_1 = \arcsin\left[\left(\frac{(f - d)^2\big[(n_2/n_1)^2 - 1\big]}{2z(f - d) - z^2} + 1\right)^{1/2}\right] \qquad (n_1 \neq n_2). \tag{A9}$$

As is shown in section 3, the main contribution to the intensity at axial position z comes precisely from the ray which is incident under $\theta_s = \theta_1$ with θ_1 given by equation (A9).

References

[1] Török P, Varga P, Laczik Z and Booker G R 1995 Electromagnetic diffraction of light focused through a planar interface between materials of mismatched refractive indices: an integral representation *J. Opt. Soc. Am.* A **12** 325–32

[2] Wiersma S H and Visser T D 1996 Defocusing of a converging electromagnetic wave by a plane dielectric interface *J. Opt. Soc. Am.* A **13** 320–5

[3] Dhayalan V and Stamnes J J 1998 Focusing of electromagnetic waves inside a dielectric slab: I. Exact and asymptotic results *Pure Appl. Opt.* **7** 33–52

[4] Wolf E 1959 Electromagnetic diffraction in optical systems. I. An integral representation of the image field *Proc. R. Soc.* A **253** 349–57

[5] Richards B and Wolf E 1959 Electromagnetic diffraction in optical systems. II. Structure of the image field in an aplanatic system *Proc. R. Soc.* A **253** 358–79

[6] Wiersma S H, Török P, Visser T D and Varga P 1997 Comparison of different theories for focusing through a plane interface *J. Opt. Soc. Am.* A **14** 1482–90

[7] Ling H and Lee S-W 1984 Focusing of electromagnetic waves through a plane interface *J. Opt. Soc. Am.* A **1** 965–73

[8] Stamnes J J 1986 *Waves in Focal Regions* (Bristol: Hilger) ch 8 and section 16.2

[9] Jiang D and Stamnes J J 1998 Focusing of two-dimensional electromagnetic waves through a plane interface *Pure Appl. Opt.* **7** 603–25

[10] Jiang D and Stamnes J J 1998 Theoretical and experimental results for two-dimensional electromagnetic waves focused through an interface *Pure Appl. Opt.* **7** 627–41

[11] Born M and Wolf E 1991 *Principles of Optics* 6th edn (Oxford: Pergamon) ch 3, pp 113–7

[12] Török P, Varga P and Németh G 1995 Analytical solution of the diffraction integrals and interpretation of wave-front distortion when light is focused through a planar interface between materials of mismatched refractive indices *J. Opt. Soc. Am.* A **12** 2660–72

[13] Sheppard C J R and Gu M 1991 Aberration compensation in confocal microscopy *Appl. Opt.* **30** 3563–8

[14] Török P, Varga P, Konkol A and Booker G R 1996 Electromagnetic diffraction of light focused through a planar interface between materials of mismatched refractive indices: structure of the electromagnetic field II *J. Opt. Soc. Am.* A **13** 2232–8

[15] Visser T D and Oud J L 1994 Volume measurements in three dimensional microscopy *Scanning* **16** 198–200
[16] Török P, Hewlett S J and Varga P 1997 The role of specimen-induced spherical aberration in confocal microscopy *J. Microsc.* II **188** 158–72
[17] Mandel L and Wolf E 1995 *Optical Coherence and Quantum Optics* (Cambridge: Cambridge University Press) section 3.3
[18] Gan X, Sheppard C J R and Gu M 1997 Effects of Fresnel diffraction on confocal imaging with an annular lens *Bioimaging* **5** 153–8